The use of hyper-temporal NDVI images to assess variation in factor C for the prediction of soil loss

Johanna Ngula Niipele
March, 2010

The use of hyper-temporal NDVI images to assess variation in factor C for the prediction of soil loss

By: Johanna Ngula Niipele

Thesis submitted to the International Institute for Geo-information Science and Earth Observation in partial fulfilment of the requirements for the degree of Master of Science in Geo-information Science and Earth Observation, Specialisation: Natural Resource Management

Thesis Assessment Board

Chair:	Prof. Dr. Ir. E.M.A. Eric Smaling
External Examiner :	Dr. B.G.J.S. Sonneveld
Supervisor:	M.Sc. Andre Kooiman

ITC

**INTERNATIONAL INSTITUTE FOR GEO-INFORMATION SCIENCE AND EARTH OBSERVATION
ENSCHEDE, THE NETHERLANDS**

Abstract

The process of soil loss is induced by many factors including the interactions between human activities and the natural environments, which cause impacts on both social and natural ecosystems. Soil loss resulting from water erosion is a problem that has been widely researched over the years. However, numerous methods developed to find alternative means of predicting soil loss lack the capability to dynamically predict temporal variation in soil loss. Therefore improved methods of predicting soil loss are required to improve traditional methods of estimating factor C used as input in soil prediction models.

The objective of the study was to assess the use of MODIS Hyper-Temporal NDVI imagery in estimating factor C.

Factor C was calculated from ground and canopy cover factors estimated in the field. Field data collection was carried out during the dry season, thus canopy cover estimations were low as compared to the average NDVI values over a 10 year period. Vegetation cover in the Crete Island is dominated by mountain phragana and grass steppe amongst others. However it is assumed that the present vegetation cover types represent centuries of soil loss. The resulting factor C was correlated to the average NDVI values of January and September over ten years period. Satellite remote sensing through hyper-temporal image analysis was used as it has the capability of matching temporal scales of assessing variations in factor C estimated for MODIS imagery.

The analysed results showed that there is no relationship between field calculated factor C and MODIS NDVI.

Acknowledgements

Words alone cannot express the gratitude I feel within and expressing myself has always been a challenge, and even today when a dam of words is flooding within me I cannot find a better way of showing my appreciation. All I can say is thank you. To my first supervisor Mr. Andre Kooiman, thank you for your guidance, sincerity and understanding. You have made me believe when I had no hope and made me stretch beyond my reach.

To my second supervisor Dr. Kees de Bie, thank you for your patience and guidance. And maybe this is a better platform for me to tell you that, every time you saw me smile, it was a smile of uncertainty. But that aside, you have build my confidence and made me believe that nothing is impossible.

To Dr. Michael Weir, I don't know how to even begin expressing my appreciation. For the past 18 months that I have been around, I have come to know you not only as an academic, but as a psychologist as well. There were times when the going got tougher and the temptation of giving up was reigning high, but your encouragements and concerns would not let us give up, at least not without a fight. And now today, I have come to appreciate the struggle I went through.

To Mr. Amjad Ali, thank you so much for dedicating your time to lend a hand. I wish you all the best in your future endeavours.

And finally a special thanks to my parents who took on my every responsibility for the past 18 months, I am indebted to you forever. You are my backbone, my shield and my life.

Table of contents

List of figures

List of tables

Abbreviations

ALOS	Advanced Land Observing Satellite
C_C	Canopy cover factor
C_G	Ground cover factor
C_{Res}	Residual land use factor
C_{Re}	Reconsolidation factor
C_{OM}	Organic matter factor
EO	Earth Observation
ISODATA	Iterative Self-Organizing Data Analysis
MODIS	Moderate Resolution Imaging Spectroradiometer
NIR	Near Infra Red
NDVI	Normalized Difference Vegetation Index
R	Red
USLE	Universal Soil Loss Equation

1. Introduction

1.1. Soil loss

Soil loss is caused by a process by which earth materials are transported away from the original location across a given surface Lorent et al. (2008). The process of soil loss is induced by many factors including the interactions between human activities and the natural environments, which cause impact on both social and natural ecosystems Lorent et al. (2008). Human induced activities such as extensive livestock keeping and crop production, has lead to a decrease in vegetation cover as natural vegetation is removed to give room to fields for crop production as well as rangeland areas Verheijen et al. (2009) and López-Bermúdez et al. (1998). Climatic conditions are part of external factors that influence the loss of soil when heavy rainfall occurs at the end of extensive dry seasons.

Concepts developed over the years, were used to combine various variables for calculating physical measurements of soil loss based on specific sites and field conditions Wischmeier et al. (1978). These variables were grouped under six major factors defined as: measured amount of eroded material (factor A), rainfall (factor R), soil erodibility (factor K), slope-length (factor L), slope steepness (factor S), land cover (factor C), and support practice (factor P). Each of these factors in itself is a function of several secondary variables or sub factors. The integration of these factors is expressed as: A=R*K*L*S*C*P used for soil loss prediction (Kooiman 1987) and (Gumiere, Le Bissonnais et al. 2009). The Universal Soil Loss Equation (USLE) factors are not free from errors especially when the equation is used elsewhere apart from United States. Limitations in the equation are due to the fact that it fails to estimate gross soil loss and also it lacks the capability of computing deposition along hill slopes, depressions and in valleys (Saavedra 2005). The equation is not event-based and lacks the means to classify events likely to occur in large-scale erosion (Merritt, Letcher et al. 2003).

1.2. Rainfall

Rainfall factor plays an important role in soil loss and must be considered at all times when assessing a water erosion problem. This is because the movement of soil particles by rainfall is usually greatest and most noticeable during short and highly intensive rainfall duration, while erosion caused by long lasting and less intense rainfall events is not easily noticeable (http://www.omafra.gov.on.ca/ ; Damen 1991; Saavedra 2005).

The R factor in the USLE is usually calculated from monthly and annual precipitation data and defines rainfall erosivity as the aggressiveness of the rain to cause erosion. The R factor is considered to be highly correlated to soil loss. (Kouli, Soupios et al. 2009).

1.3. Soil erodibility factor

Soil erodibility factor K, refers to the inherent properties of the soil to erode at different rates due to differences in soil properties which are determined by land cover types and land use activities in specific areas (Wischmeier and Smith 1978; Mainam 2000). Soil erodibility depend on infiltration capacity and the capacity of soil particles to resist detachment (Mainam 2000). The resilience of soil to detachment depends on the topographic position and slope steepness. It is also influenced by soil roughness which is an indicator for the degree of clodiness and the likelihood that the soil surface will seal, producing an increased runoff leading to soil erodibility. Also, the amount of disturbance created by human activities, such intensive animal grazing and agricultural land use are of most importance in determining the amount of soil loss in an area (Institute of Water Research 2007).

1.4. Vegetation cover

Different vegetation cover and structures are known to provide protection to soil from rainfall intensity. The degree of protection depends on the vegetation structure and its canopy (De Bie 2005), thus creating a relationship between percentage ground cover and the reduction of soil loss. The canopy protection of vegetation does not only depend on the type of vegetation and its characteristics, but also depends on the variability between different months or seasons (Wischmeier and Smith 1978).

Factor C is the cover factor used to reflect the effect of vegetation and ground cover on the rates of erosion. A value of factor C representing a specific cover type signifies a percent of the amount that erosion will be reduced under that specific cover type (Institute of Water Research 2007). The concept of computing factor C is adopted from the USLE (Universal Soil Loss Equation) and RUSLE (Revised Universal Soil Loss Equation), which uses a sub-factor method to compute soil loss ratios. The amount of soil loss ratios vary with time based on vegetation canopy, ground cover and soil roughness. A factor C value is an average soil loss ratio weighted according to the distribution of rainfall (R) during the year. For the purpose of this study, the sub-factors used to compute soil loss ratio values are canopy cover and ground cover, based on current and previous land uses (Institute of Water Research 2007). However the rainfall factor (R) which is an important component in water based erosion is not used due to lack of relevant data used for that purpose.

Factor C accounts for ground and canopy cover effects on soil loss. Canopy cover is based on the vegetation cover definition, which is the aerial cover of the highest vegetation layer and basal cover which is the proportion of ground surface percent under vegetation at mowing height, De Bie (2005).
Factor C is expressed as [CC*CG*CRes*CRec*COM], where:

CC = canopy cover factor – canopy cover is all types of vegetation including crop types. The canopy of vegetation cover has an influence on the erosivity of the total amount of rain that intercepts the canopy and the rainfall that reaches the soil surface. The magnitude of the through-fall and stem-flow effects depends on the canopy percentage cover, height, size, position and shape of leaves Kooiman (1987) and De Bie (2005).

CG = ground cover factor – ground cover includes, litter, basal cover and stones. It slows down overland flow by protection soil against splash thus detaining water long enough to allow infiltration (De Bie 2005).

CRes = residual land use factor – residual land use refers to the former land cover and land use on the present erodibility of the soil. It may account for forests or long term grasslands, that have a relatively strong effect and long duration, but also for shorter fallows and temporal cover crops, Kooiman (1987).

CRec = reconsolidation factor - reconsolidation is explained by the development of erodibility following Landuse changes and the changes that appear after land abandonment, Kooiman (1987).

COM = organic matter factor - organic matter is explained by the amount of organic matters in the soil from the remains of previous land cover and land use materials, which decreases the effect of erodibility Kooiman (1987) and De Bie (2005).

The cover factor C is calculated from field observed vegetation canopy cover and ground cover percentage estimates. Vegetation canopy cover is generally estimated from the normalized difference vegetation index (NDVI) assuming a linear relation which is not always the case, as surface cover does not only include vegetation canopy cover but also plant residue (litter) and ground cover. (Suriyaprasit and Shrestha 2008)

Ground cover is defined as the material in contact with the soil surface that intercepts raindrops and slows surface runoff. This includes all cover types present, including rock fragments, live vegetation, and plant residue (litter). The total percent of ground cover is thus used to compute how surface cover affects erosion (Institute of Water Research 2007). Ground cover has been found to have a strong influence on the effect of reducing soil loss and the degree of protection differs between cover types. For example, rock fragments have been found to decrease run-off yield by scattering the impact energy of a raindrop, in thus interfering with the movement of water and in the process allowing a high infiltration rate. Also the effect of plant residue (litter) on soil surface acts as a residual cover, which protects soils from direct impact of raindrops thus slowing down water run-off and increasing infiltration rate (Kooiman 1987; Nyakatawa, Reddy et al. 2001).

A number of dynamic models have been developed for predicting soil loss. However predictive models require land cover/land use and canopy cover information in order to run. Vegetation canopy cover information is crucial in this regard as it gives information on rain interception factor, both of which are important input in calculating runoff and soil loss. Obtaining such data is not always easy especially in mountainous areas because of inaccessibility problems. In this regard remote sensing data became very important. (Suriyaprasit and Shrestha 2008)

1.5. Land use

In human-dominated domain such as agricultural landscapes, land degradation and habitat fragmentation depends very much on the spatial and temporal pattern of disturbance (Pueyo, Alados et al. 2006). The ever increasing population has led to a higher demand for more agricultural land and grazing areas. This has led to land degradation and habitat fragmentation as an influence from forest fires, overgrazing and intensification on agricultural areas. The intensification of livestock and agricultural production has caused variation in land use types and turned what was once characterised by a great variety of natural features into degraded landscapes (Arianoutsou 2001). Forest fires, act as a generalist herbivore of removing plant material above the ground surface, which enable new herbaceous growth much preferred by grazers and browsers. However the effect of fire exposes bare soil to weathering processes which can lead to soil loss due to a decrease in vegetation cover which plays a major role in the protection of bare soils (Saavedra 2005; Lorent, Evangelou et al. 2008).

1.6. Time

Soil loss ratios vary during the year and the effectivity of vegetation cover depends on the combination of plant development and rainfall intensities in different periods of the year. Values for C are calculated on the base of rainfall distribution over the year and on the different stages in plant development. These can be assessed in crop calendars and time series of NDVI values. The effectivity of crop cover in different periods of vegetation development is thus related to the relative erosion index (Ei30) percent during those periods (Kooiman 1987).

1.7. Remote Sensing

Advances in Earth Observation (EO) technology have brought about new development of retrieving information to assess environmental processes. The use of high spatial resolution and advanced image processing techniques had led to improvements in the assessment of soil loss (Karydas, Sekuloska et al. 2009). Moreover, satellite remote sensing through hyper-temporal image analysis may allow us to match temporal scales of assessing soil loss from factor C derived from Moderate Resolution Imaging Spectroradiometer (MODIS) Normalized Difference Vegetation Index (NDVI). And this could be related to factor C calculated from field observations, thus making it possible to determine temporal variation between processes of different soil loss parameters, and in turn improving soil loss prediction modeling techniques (Yang and Liu 2005).

To date few studies have assessed long-term trends in NDVI index values using remote sensing data. A method developed by Gitas (2009) on the use of Multi-temporal NDVI data has bridged the gap of classifying temporal variations in soil erosion processes. This had led to the assumption that hyper-temporal images may further improve the method by classifying variations in factor C derived from MODIS NDVI values as inputs in soil loss predictions.

1.8. MODIS hyper-temporal NDVI

MODIS offers 16-day NDVI composites with 250*250 m spatial resolution in the red and near infrared channels. The sensor provides a coverage that can be used in land cover mapping at a finer scale. (Karlsen, Tolvanen et al. 2008). NDVI is defined as (NIR-R)/ (NIR+R), where NIR is the reflectance measured in near infrared and R is represented by the red channels. NDVI provides an effective measure of photosynthetically active biomass which is a measure of concentrated chlorophyll in plant tissues (measure of vegetation greenness).

The application of NDVI was employed in the study as it is able to detect biomass fluctuation over time, thus suitable in the studies of vegetation phenology and landscape degradation. More importantly, its effectiveness extends to cases of limited data availability and situations of inaccessible areas (Ali 2009).

NDVI effectively provides us with information on the spatial and temporal distribution of vegetation as well as on the abundance of vegetation communities. (Pettorelli, Vik et al. 2005; Scarrott 2009)

Hyper-temporal imagery refers to images acquired at a fixed time at a high temporal resolution using different time periods of the same time. MODIS NDVI is such data and thus creates an opportunity to allow the extraction of information on temporal variation in land cover and vegetation conditions.

2. Research approach

2.1. Justification and problem definition

Over the years several methods have been developed to assess and predict average annual soil loss, but most of these methods lack the ability to dynamically predict temporal variation in the rate of soil loss. Also most soil prediction models use data derived by using calculations based on the original USLE by Wischmeier (1978). However the USLE has limitations in that factor C is calculated from specific land use types and areas of certain management practices and environmental conditions (Wischmeier and Smith 1978). New methods are thus required to improve traditional ways of predicting soil loss as old methods fail to account for temporal variation in soil loss processes and also fail to put into consideration field calculated factor C from natural environments.

Factor C is calculated from field based data using the USLE as outlined in the previous chapter. What is not known is how to estimate cover percentages taking into account seasonal variations. Traditional methods require multiple field observations in order to estimate cover percentages, therefore a need to improve these methods. New methods need limited field observations to calculate factor C and also to detect temporal variation in the rate of soil loss. It is for these reasons that the study aims to test the effectiveness of hyper-temporal MODIS NDVI in calculating factor C, as it is readily available at no cost, yet having the ability to predict temporal variation. Hyper-temporal NDVI dataset will give us timely information on the rate of soil loss and this will be useful to soil conservationists, environmental managers and agencies.

Recently, hyper-temporal remote sensing data have been made available and could be used to directly estimate factor C from above in turn reducing extensive fieldwork traditionally needed to calculate factor C.

The aim of the study is to test whether hyper-temporal NDVI data can be used to estimate factor C used as input data in soil loss prediction models. This was done by relating NDVI values to land cover types based on field observations.

2.2. Research objective

The objective of the study is to assess the use of MODIS hyper-temporal NDVI images to estimate factor C as input for soil loss prediction.

2.3. Research question

One research question has been developed to help us answer the research objective:
Does MODIS NDVI data correlate to field calculated factor C?

2.4. Hypothesis

Ho: There is no significant relationship between MODIS NDVI and field calculated factor C
Ha: There is a significant relationship between MODIS NDVI and field calculated factor C

3. Methodology

3.1. Study area

The Crete Island in Greece is characterised by mountainous landscapes, where various calcareous rocks (limestone and dolomites) dominate the mountain terrain (Shrestha, Zinck et al. 2004), and neogene sediments including limestone, sandstone and marls, cover large areas of the lowlands (Sarris, Karakoudis et al. 2005). The climate is sub-humid to humid Mediterranean characterised by an annual rainfall of approximately 900 mm, which decreases from west to east and from north to south (Sarris, Maniadakis et al. 2005; Kouli, Soupios et al. 2009).

Land use is characterised by agriculture in low lying areas and livestock grazing (Ouled Belgacem and Papanastasis 1995) in higher altitudes (1000-2000 m). Olive groves and grape vines dominate the agriculture system and plantations are either used for household or commercial production, while small stock as sheep and goat are primarily dominating the livestock industry (Hill, Hostert et al. 1998).

Vegetation cover is mainly mountainous phrygana, relict kermes oak forests (Hill, Hostert et al. 1998) and grass steppe which is mainly found on more gradual slope and in calcareous substrate increasing towards higher elevations (Alodos, Pueyo et al. 2004).

Intensification of traditional livestock husbandry, increasing wild fires as well as agricultural activities has led to soil loss in the Island due to inadequate land use management practices (Andel, Zangger et al. 1990; Hill, Hostert et al. 1998).

Figure 1: Map of the study area, the Crete Island in Greece. Source: Google images

3.2. Remote sensing data used

MODIS NDVI data from 18 February 2000 to 28 July 2009 were used to assess variation in factor C from above. The dataset was obtained from (http://www.landcover.org/data/ndvi/)

Table 1: Spectral bands for the MODIS dataset.

Band number	Central wavelength [nm]	Bandwidth [nm]	Spatial resolution [m]
1	645	620 - 670	250
2	858.5	841 - 876	

ALOS imagery was used in the designing of the field sampling scheme. The imagery was used as a base for stratified random sampling in the field, by identifying different image characteristics at each of the 29 randomly selected points. The selected areas from the 29 randomly selected points were then used for field observations. In addition, the imagery was used for visual interpretation whereby ten land cover classes were identified and digitized based on the image characteristics (fig. 12 and 13). The ten class units were digitized within MODIS pixels that contained each of the 29 randomly selected sample points. These class units were established in order to gain an overview of the different variations within the MODIS pixels. The resulting digitized classes were converted into signature files and used to classify the whole ALOS image.

Table 2 below shows the information of the ALOS imagery used within the context of the study.

Table 2: Band information and scenes for the ALOS dataset used (http://www.alos-restec/ 2009)

<table>
<tr><th colspan="2">AVNIR-2 Characteristics</th><th>Scene dates</th></tr>
<tr><td>Number of Bands</td><td>4</td><td rowspan="3">2009-07-09 AV2A184132890
2009-07-09 AV2A184132900
2009-07-14 AV2A184862880
2009-07-14 AV2A184862890
2009-07-26 AV2A186612890
2009-07-26 AV2A186612900
2008-05-09 AV2A121992890
2008-11-04 AV2A148102890</td></tr>
<tr><td>Wavelength</td><td>Band1: 0.42-0.50 micrometers
Band2: 0.52-0.60 micrometers
Band3: 0.61-0.69 micrometers
Band4: 0.76-0.89 micrometers</td></tr>
<tr><td>Spatial Resolution</td><td>10 m (at Nadir)</td></tr>
</table>

3.3. Methodological overview

The research approach was carried out in three steps as outlined in figure 2 below.

- Hyper-temporal image analysis
- Sampling scheme
- Product assessment

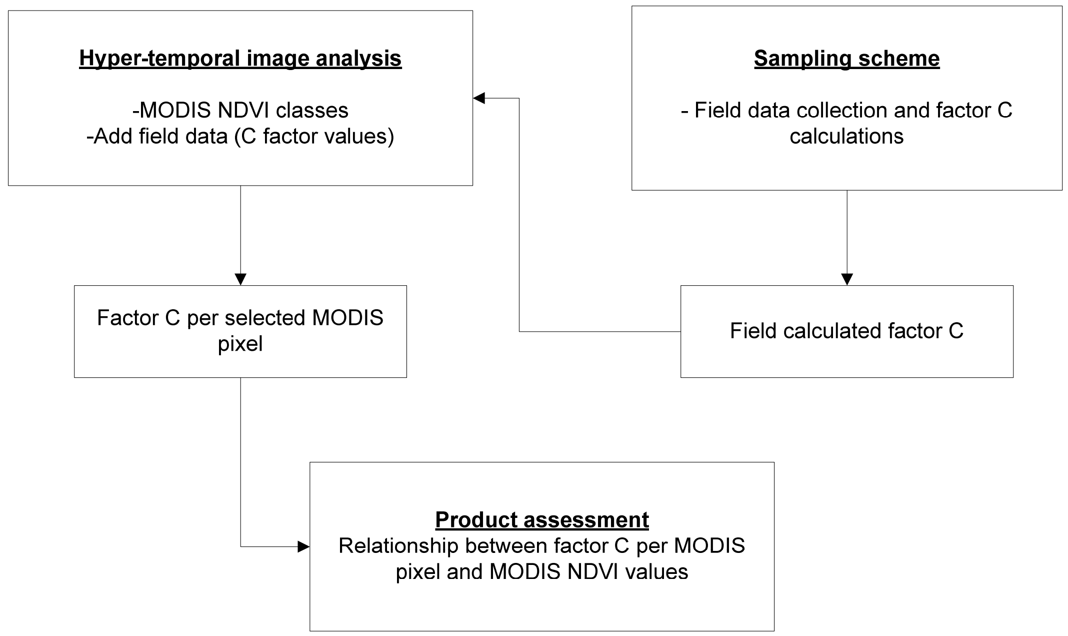

Figure 2: Schematic diagram summarizing methodological steps for the study.

Figure 3 below shows a detailed description of the methodological steps followed to achieve the objective of the study.

- Step 1, was to calculate factor C from field estimated ground cover and canopy cover sub-factors.
- Step 2, was the up-scaling of field calculated factor C to the MODIS pixels. This was done by first running a visual interpretation of the ALOS imagery, then digitizing the interpreted class units and classifying of the whole ALOS imagery based on the interpreted units.
- Step 3 was the product assessment phase, looking at relations within and between groups of MODIS NDVI classes. This was done by grouping NDVI class profiles and relating them to factor C.

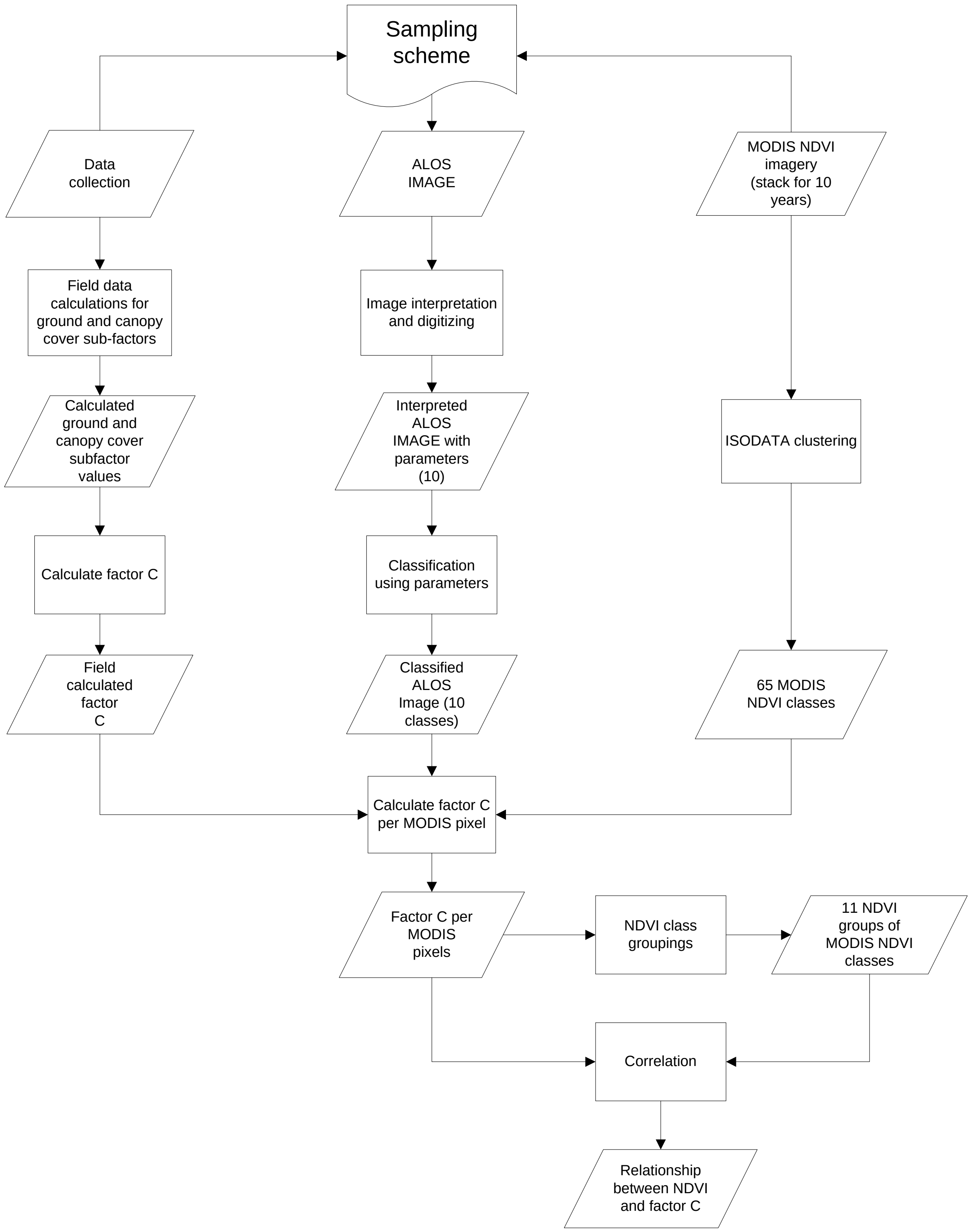

Figure 3: Methodological steps of how the study was conducted.

3.4. Hyper-temporal MODIS NDVI data analysis

Hyper-temporal MODIS NDVI imagery were analysed using an unsupervised classification method. The technique used was the Iterative Self-Organizing Data Analysis (ISODATA) algorithm, used to classify objects within a feature space by grouping similar objects within the same proximity (De Bie, Khan et al. 2008; Beltran-Abaunza 2009). Through this process a pre-defined number of 65 classes were obtained for the hyper-temporal MODIS NDVI imagery of 2000 to 2009. The unsupervised classification has been run for a predefined number of 10 to 100 classes and used to generate pre-defined NDVI classes which were used to design the field data collection materials. The iteration was set to 50 and the convergence threshold at 1 (De Bie, Khan et al. 2008). The NDVI-profiles of identified classes were extracted to excel for the analysis in order to give an overview of the minimum and averaged values for all classes.

The ISODATA clustering algorithm is an iterative procedure which assigns arbitrary initial cluster vector and classifies each pixel to the closest cluster. The procedure is repeated until the "change" between the iteration is small. The "change" can be defined in several different ways, either by measuring the distances the mean cluster vector have changed from one iteration to another or by the percentage of pixels that have changed between iterations (2010).

3.5. Sampling scheme

The sampling scheme was developed from the CORINE land cover classes, MODIS NDVI classes and ALOS imagery. CORINE land cover classes were based on the CORINE Land Cover Map of 2000 (CLC2000) (CEH 2009). The CORINE land cover classes representing agricultural and natural areas were selected for the sampling scheme. These land cover classes were used to identify NDVI classes corresponding to natural and agricultural areas as well as areas used for grazing.

Areas depicting bare rocks, water features, build up areas and coastal areas as well as areas smaller than 20 km2 were excluded from the selection. The final selection was based on agricultural areas, semi-natural and natural vegetated areas.

A total number of 29 sampling points were randomly selected based on the available number of field days (15 days). A 50 m buffer area around sampled units was established with a 1000 m distance between sampled units.

3.5.1. Field data collection

Data collection was conducted between the 22nd September and 11th October 2009. 29 Points were randomly selected and overlaid onto the MODIS NDVI grid and ALOS imagery. The resulting images where loaded onto the IPAQ device and a hard copy printed to be used for data collection. Once the sample points were located in the field, the printed hard copy was used to identify surrounding areas that showed variations on the ALOS imagery within the MODIS classes. Depending on the identified number of variation from the ALOS imagery, group members either grouped up or individually visited the identified areas and collected the required data. The 29 randomly selected points formed clusters, were a total number of 111 observations were collected.

Field data collection included collecting vegetation biophysical attributes (ground cover, vegetation structure and canopy cover), erosion features and grazing parameters in natural areas. In order to cover full vegetation classes, the sampling scheme was modified, whereby sampling units were selected based on the variation of MODIS classes and ALOS image characteristics. Figure 4 below, show points representing the 111 observations carried out within the 29 randomly selected points.

Although attributes relating to erosion features, infiltration capacity and grazing indices were collected, this information was not used further in the analysis as they were irrelevant to the objective of this study. Therefore these dataset was ignored.

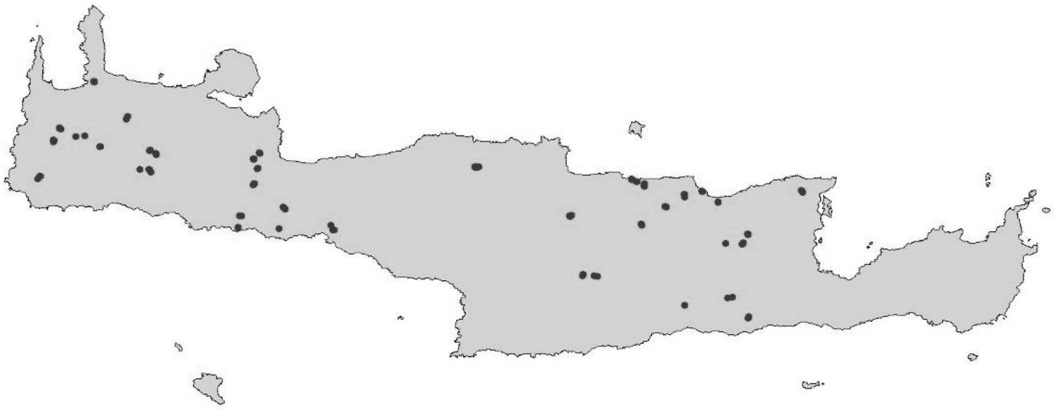

Figure 4: Map of the study area showing sampled points.

Ground cover

Ground cover parameters included percent cover by stones, litter, basal cover (for live vegetation) and bare soil at the sampled points. Data collection was based on visual estimation of different ground cover parameters by the observer (s) within a 30*30 m quadrate.

Vegetation structure

The information on vegetation structure was based on field observations, whereby information related to vegetation such as percent of canopy cover in different layers, biomass density and dominant species were estimated. Different vegetation structural layers, average height and the percentage cover per layer were recorded as indicated in figure 5.

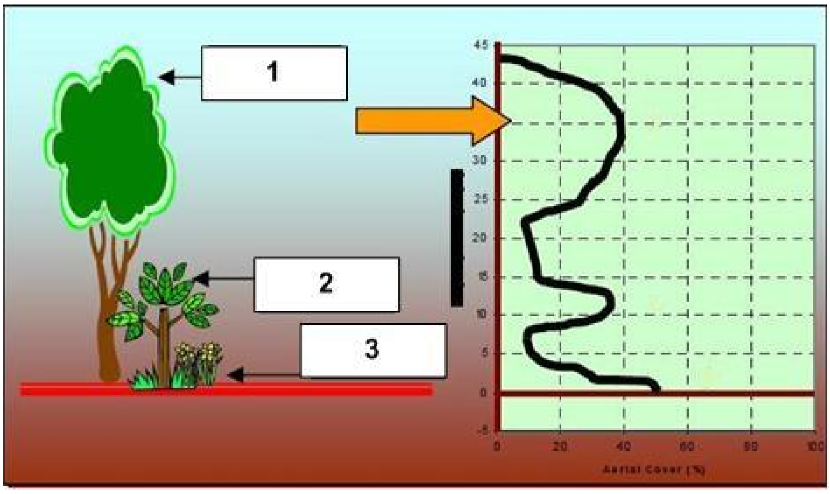

Figure 5: Vegetation structural layers as perceived in the field. (Source: de Bie, 2000)

3.5.2. Factor C calculations

Data preparation and analysis were carried out in ArcView, ArcGIS, ENVI, ERDAS, SPSS and Microsoft Excel softwares.

Factor C as expressed by Wischmeier and Smith (1978); Kooiman (1987) and De Bie (2005) was calculated by multiplying factors that have an influence on soil loss such as ground and canopy cover effects. The original formula by Wischmeier and Smith (1978) [CC*CG*CRes*CRec*COM] accounted for canopy cover, ground cover, residual land use, reconsolidation and organic matter factors. The focus for the study is to calculate factor C from ground cover and canopy cover factors [CC*CG] and relating it to MODIS NDVI values.

Ground cover (CG) was calculated by subtracting the sum values of the specified cover types from the total estimated ground cover percentage (100%) using the formula [100 %-(%litter + %basal cover + %stones +%water)] (source: De Bie, 2005). Alternatively it could also be computed by subtracting bare soil percentage from the total ground cover percentage [100%-%bare soil]. Ground cover sub-factor (CG) was computed by cover type using the following formula [e-(b*Ground cover (%))] (De Bie 2005), where b is a constant depending on the surface roughness of the topsoil. A value of 0.04 was substituted for roughness (b) factor assuming the entire area had medium topsoil surfaces. Ground cover percentage is low, when bare soil percentage is high. And this is an indication for areas that are vulnerable to soil loss (Damen 1991). Figure 6 (B) below is a graphic representation of ground cover sub-factor (CG) against the actual ground cover %.

Percentage canopy cover and height per vegetation layer was estimated in the field. The resulting field estimates were used to calculate canopy cover sub-factor per sample site at different vegetation structural layers, using the formula adopted from (Wischmeier and Smith 1978; Kooiman 1987; de Bie, Bouma et al. 2000): Where b = (Ymax-1)/100, representing maximum canopy sub-factor at various effective average canopy heights and; Y= (b*X) +1, where Y is the canopy sub-factor (figure 6 A). Total CC sub-factor was calculated by multiplying canopy sub-factors of each layer.

The resulting canopy cover and ground cover sub-factors were used to calculate factor C from field data using the formula: Factor C = CG x CC. It should be noted that canopy cover (CC) and ground cover (CG) factors are influenced by Com, Cres and Crec. But due to limited data availability, soil erodibility sub-factor was rather excluded from the calculations for Factor C.

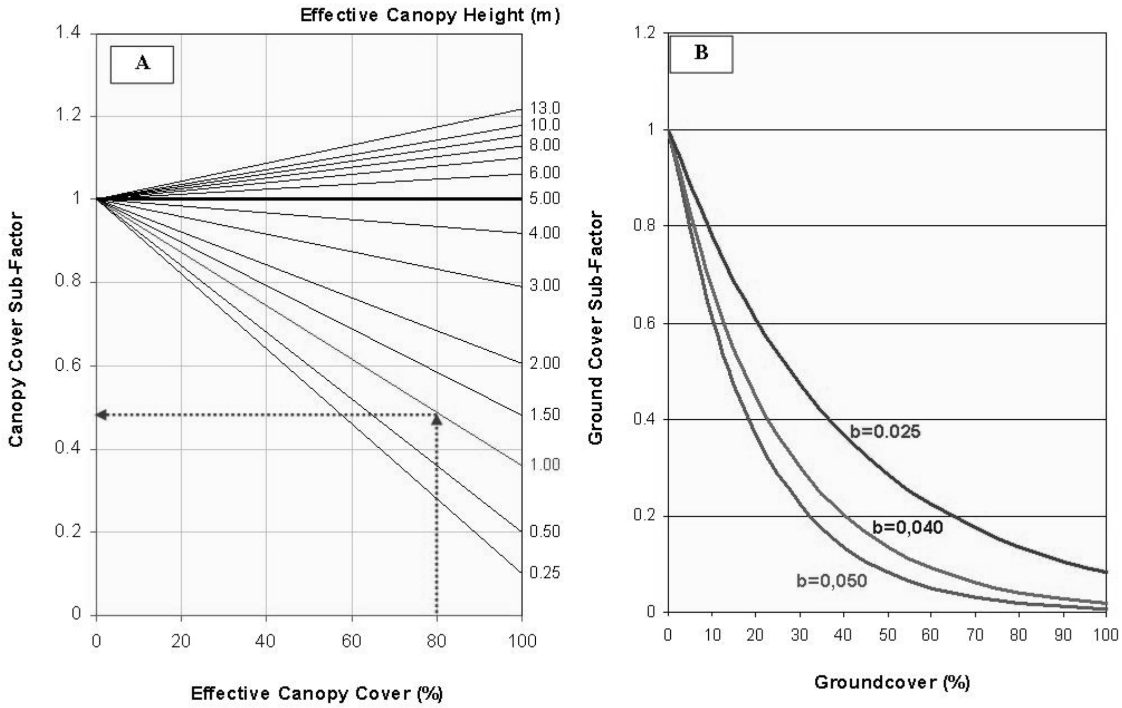

Figure 6: The assessment of canopy cover (CC) (A) and (CG) (B) factors. (Source: de Bie, 2000)

Field calculated factor C was up-scaled to MODIS pixels. Estimates for field calculated factor C were based on a 30*30 m grid area around sampled point and were not representative of the cover variation within MODIS pixels. In this regard the ALOS imagery (10*10 m resolution) was used as a base for up-scaling point based field calculated factor C to MODIS pixels. The ALOS imagery was visually interpreted and digitized based on the interpreted class units. The interpretation was limited to MODIS pixels containing the 111 points which were sampled in the field. A preliminary legend was established from the visual interpretation and used to classify the ALOS image into 10 units (A-J). Classified units were polygonized, dissolved and crossed with MODIS pixels. Areas of ALOS units within MODIS pixels were calculated and areas smaller than 100 square meters where eliminated. Furthermore a mean value for each ALOS unit was derived from field calculated factor C within each MODIS pixel. Using the formulas below, weighted factor C was calculated per unit within a MODIS pixel and summed up to give the total factor C per MODIS pixel.

Area fraction = Area ALOS unit x 100 /Area of MODIS pixel

Where area fraction is the fraction of the area covered by each ALOS unit within a MODIS pixel and area ALOS unit is the sum of ALOS units in each MODIS pixel, while the area of MODIS pixel is the total area of the MODIS pixel containing ALOS parameters; and

Weighted Factor C = Area fraction x Mean Factor C / 100.

Where weighted Factor C is the sum of fraction of ALOS units within each MODIS pixel and mean factor C is the mean value for each ALOS unit based on field calculated factor C.

It should be noted that in order to have a high degree of freedom (df), factor C per MODIS pixel was not calculated per sampled point, but for a number of selected MODIS pixels around sampled points. MODIS pixels were selected by using the stratified sampling method, whereby pixels around sampled points were identified and selected. Extracted NDVI values were than correlated to the weighted factor C.

3.6. Product assessment

Scatter plots were used to assess the relationship between field calculated factor C and MODIS NDVI. First NDVI classes representing pixels of field calculated factor C were arranged into group of similar profile behaviours. Then the classes within the group were correlated to see whether there were any relationships within and between groups of NDVI classes. Average NDVI values for January and September were used in the correlations as they represented the months with low and high NDVI values. January values represented the highest peak of vegetation greenness, while September represented the lowest peaks of vegetation greenness and the month of actual fieldwork. Profiles of NDVI land cover classes per MODIS pixel corresponding to field calculated factor C are illustrated in figures 16 to 23.

4. Results

4.1. Hyper-temporal MODIS NDVI data analysis

218 Layers of NDVI stack representing images between 18 February 2000 and 28 July 2009 were classified. Figure 7 shows the separability dates by the number of classes of the unsupervised classification results. The 65 class ran was identified as the best number of classes for divergence statistics in the ISODATA classification. The optimal number of classes is indicated with a line at the highest peak which corresponds to a signature file of the 65 classes (Beltran-Abaunza 2009). The selected classes were further used to create MODIS NDVI classes in figure 8 as well as to develop the sampling scheme for fieldwork.

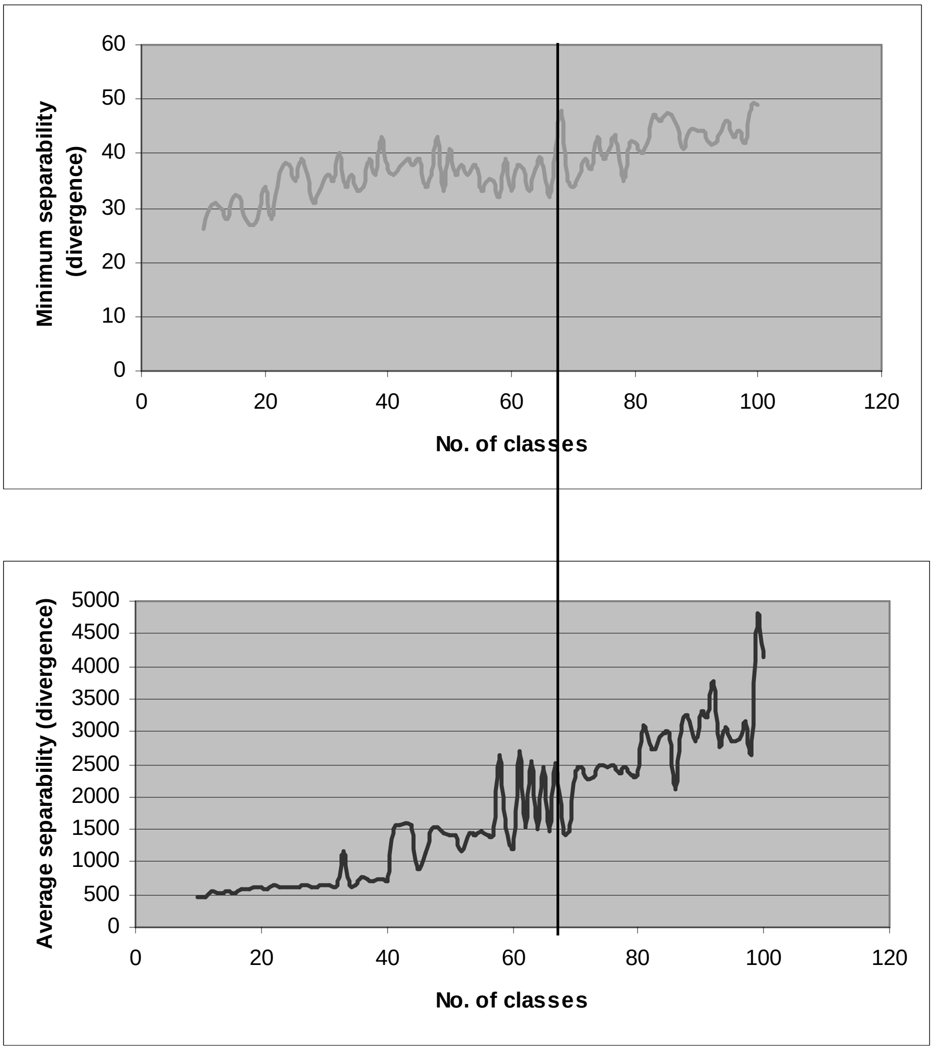

Figure 7: MODIS optimal number of classes used for the unsupervised classification.

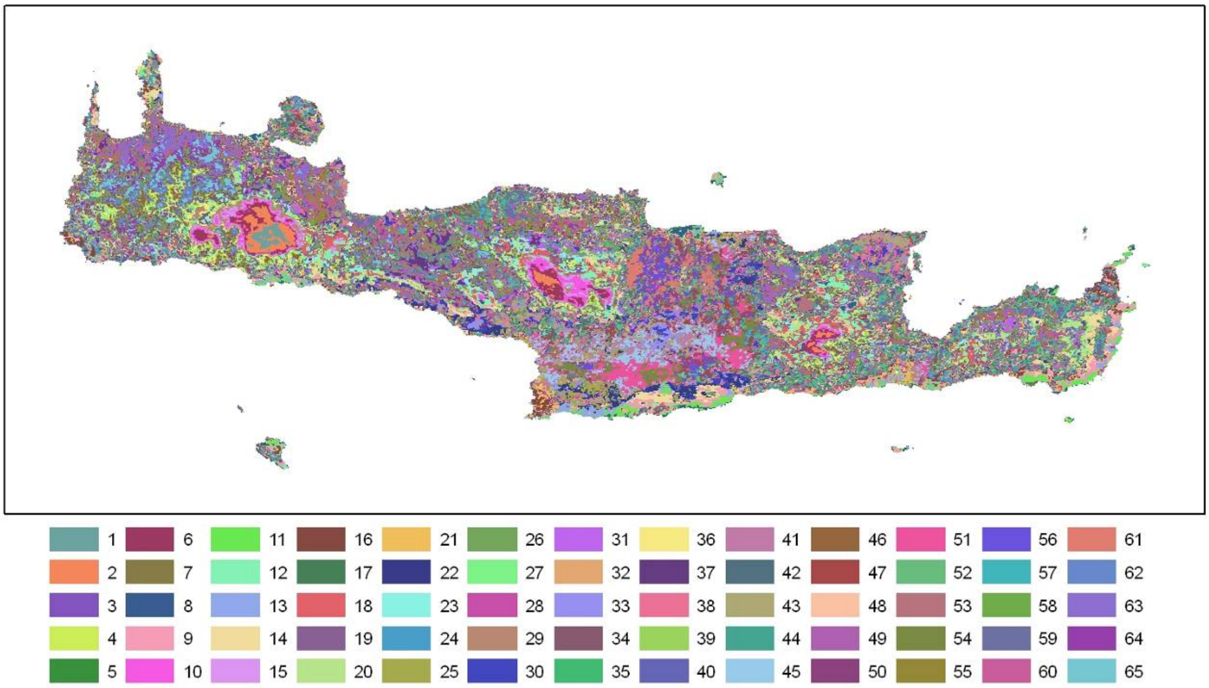

Figure 8: The 65 MODIS NDVI classes identified by ISODATA clustering.

4.2. Sampling scheme

4.2.1. Factor C calculations

Factor C was calculated for each of the 111 points observed in the field from the 29 clusters that were randomly selected using the designed sample scheme. Thereafter, field calculated factor C was up-scaled to MODIS pixels as described in section 3.5.2. However extra MODIS pixels were selected using a stratified method, whereby pixels surrounding the pixel that contained the sampled point were selected. These extra pixels were selected in order to increase the degree of freedom. Figure 9 below illustrates the method used to select extra pixels. The black square represent the pixel containing the sampled point and the white dot in the middle represents the sampled point. The grey squares represent the selected pixels surrounding the pixel within which observations were based.

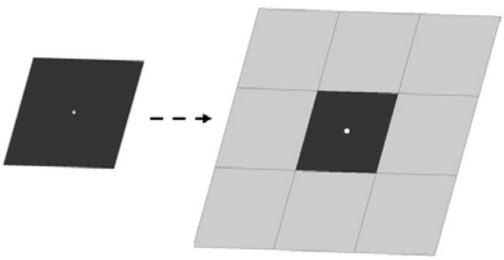

Figure 9: Example of how extra MODIS pixels were selected.

Figure 10 below illustrates the range of distribution for factor C in the selected MODIS pixels. The range was observed between 0.010 and 0.371. The highest distributed factor C was observed at the range of 0.368 and the lowest distributed factor C was observed at 0.011.

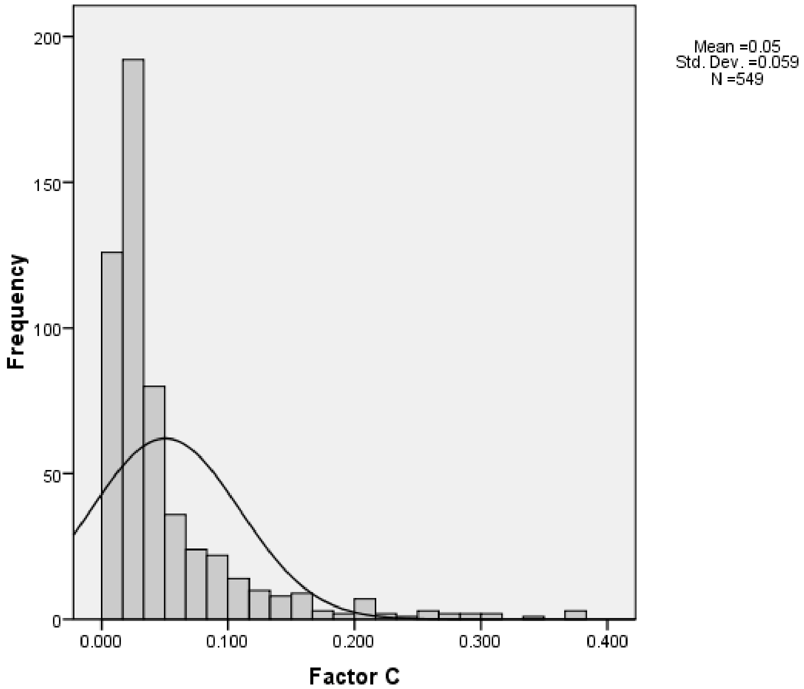

Figure 10: Histogram showing the distribution of factor C for the selected MODIS pixels.

The histogram in figure 11 shows the distribution of factor C per MODIS pixel within groups of NDVI classes. The highest distribution of factor C can be observed in group 1 representing 117 pixels. And the lowest was observed in group 10, whereby only 3 pixels were represented.

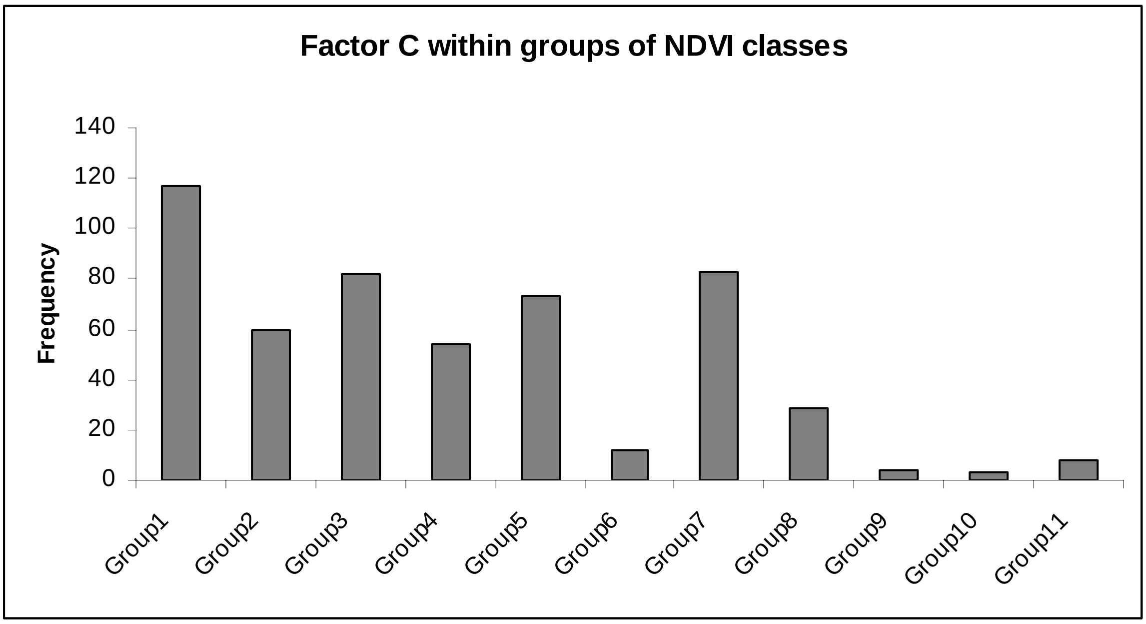

Figure 11: Histogram showing the distribution of factor C within NDVI groups.

Figure 12 below shows a classified ALOS image. The classified class units were used for up-scaling field calculated factor C to MODIS pixels. 10 class units representing variability in land cover within MODIS pixels were identified.

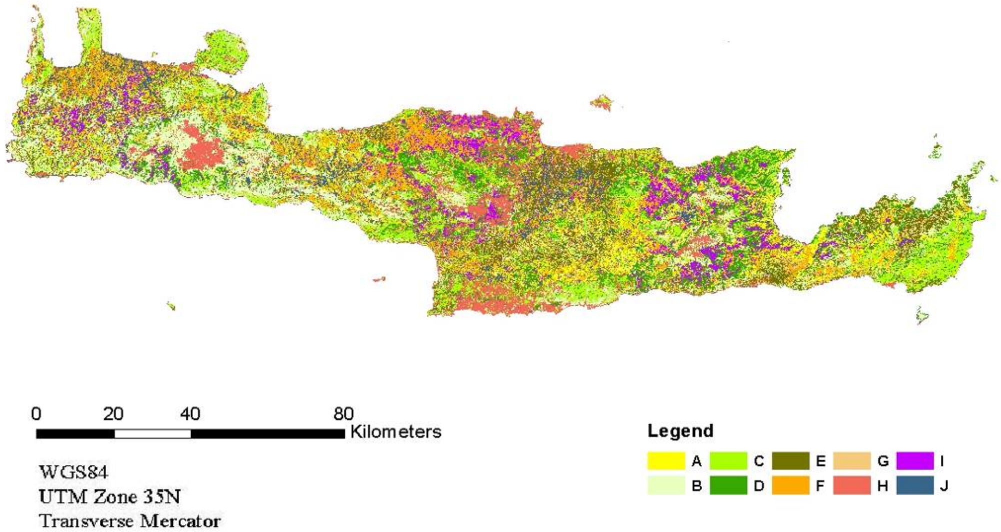

Figure 12: Map units of the ALOS classification.

ALOS class	Code colour	Mean factor C	Image	ALOS class	Code colour	Mean factor C	Image
A		0.017		F		0.051	
B		0.034		G		0.013	
C		0.027		H		0.013	
D		0.371		I		0.013	
E		0.025		J		0.068	

Figure 13: Detailed legend of factor C per ALOS class.

Figure 13 is a detailed legend of the ALOS interpreted class units. In the legend factor C per class unit is displayed with a corresponding image representing what the units look like in reality.

Fifty three (53) NDVI Classes were selected from the 65 classes generated through ISODATA clustering. The 53 represents field calculated factor C within MODIS pixels. Represented classes were grouped into profiles of similar behaviour. NDVI values related to the identified classes were visually analysed and used to select months depicting the highest (January) and lowest (September) peaks.

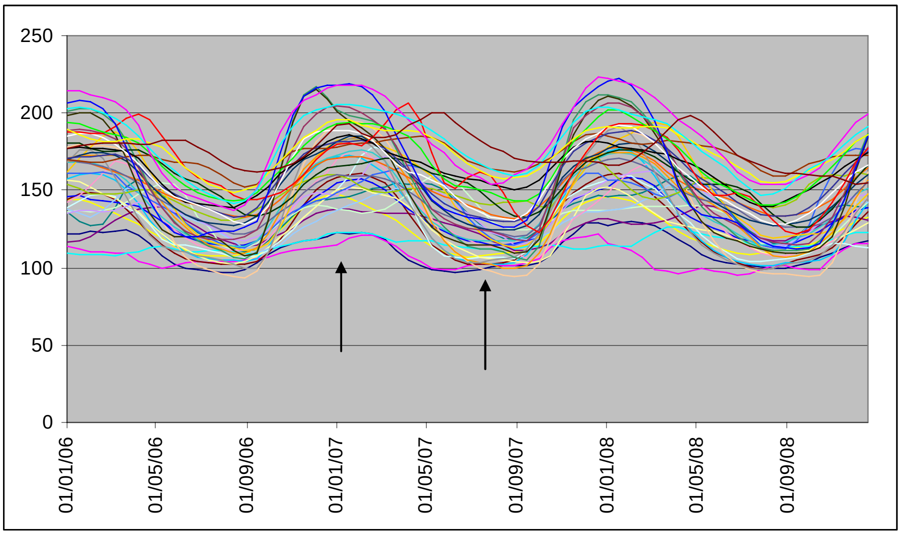

Figure 14: MODIS NDVI profiles showing high and low peaks over 10 years.

4.3. Product assessment

Relationships within and between variables were measured for groups of NDVI classes. In figure 11 below box plots were used to display the distribution of factor C within groups of NDVI classes. Group variables were displayed side by side in order to gain a quick overview of the comparison and spread of the data.

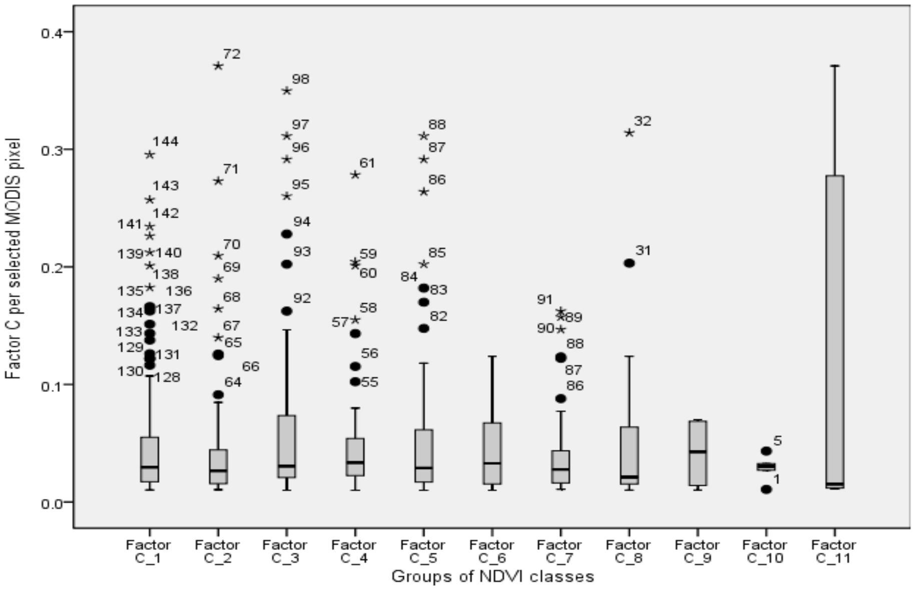

Figure 15: Distribution of factor C for MODIS pixel within groups of NDVI classes.

Scatter plots depicting factor C per MODIS NDVI class were used to display and explain the relationship between NDVI and factor C, figure 16-23. Average NDVI values for January and September over 10 year's period were correlated to factor C per MODIS pixel within groups of NDVI classes. The resulting plots are displayed in figures 16 to 23. These resulting plots demonstrate little or no correlations between NDVI and factor C. The low correlation can be due to the resolution of the MODIS NDVI imagery which has a low spatial resolution of 250*250m in relation to the 30*30m quadrate at which factor C was estimated. Factor C values relating to low NDVI values is an indication of cover protection that is not related to green biomass which could be stressed vegetation, or areas covered by other kinds of ground cover such as litter and stone.

Figure 16 shows the distribution of factor C in group 1 ranging between NDVI values of 90 and 210 for January and between 80 and 190 for September. Classes depicting low factor C values were observed at the extreme ends of the plots. Low factor C values indicate less potential for soil loss taking place within these classes. The range of values scattered in the centre of the plots, indicate classes that have potential for soil loss. This range also indicates that MODIS NDVI is unable to detect changes in factor C.

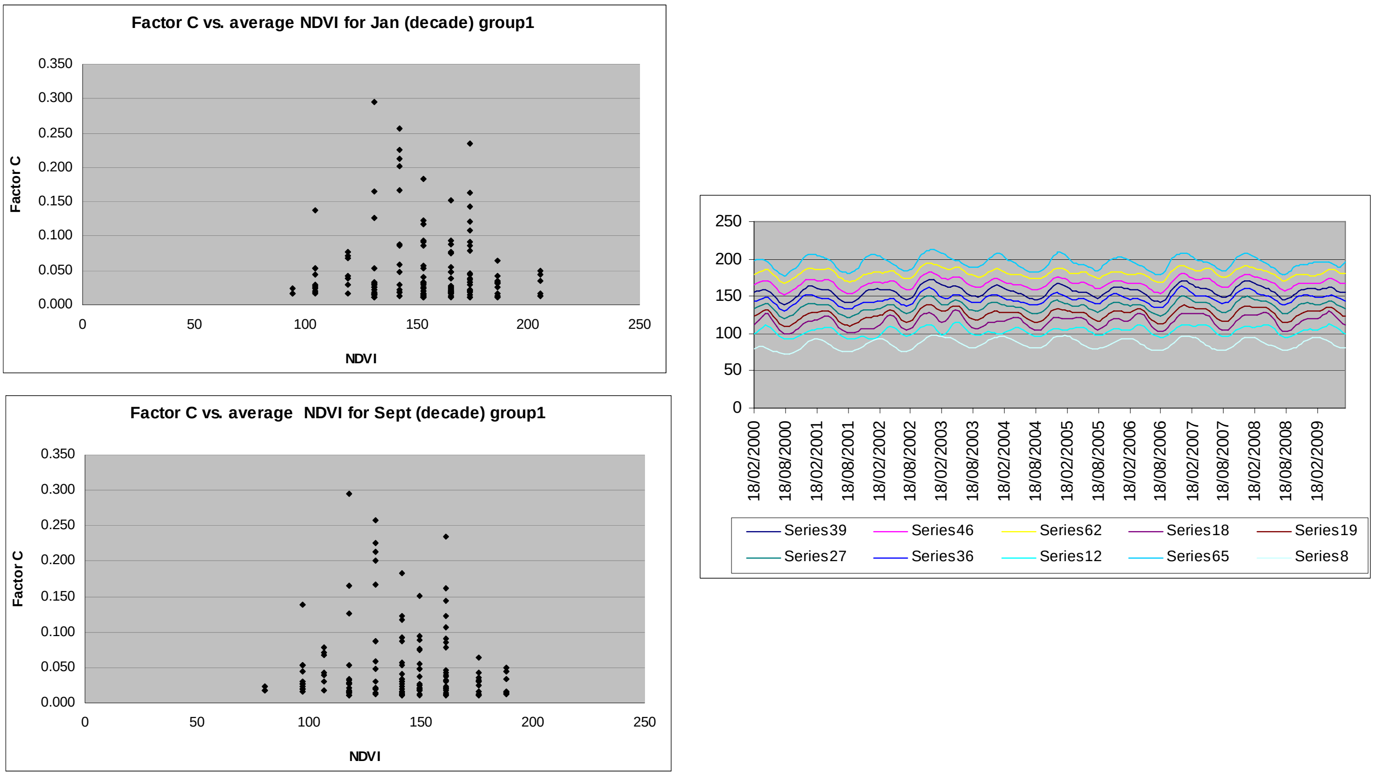

Figure 16: Relationship between factor C and NDVI for group 1.

Figure 17 shows the distribution of factor C in group 2. NDVI values ranges between 160 and 215 for January and within a range of 90 and 175 for September. The lowest value for factor C is found at NDVI value of 215, meaning that there is a relatively low potential for soil loss taking place. A high factor C at the lowest NDVI value 105 was observed, indicating that there was no high potential for soil loss.

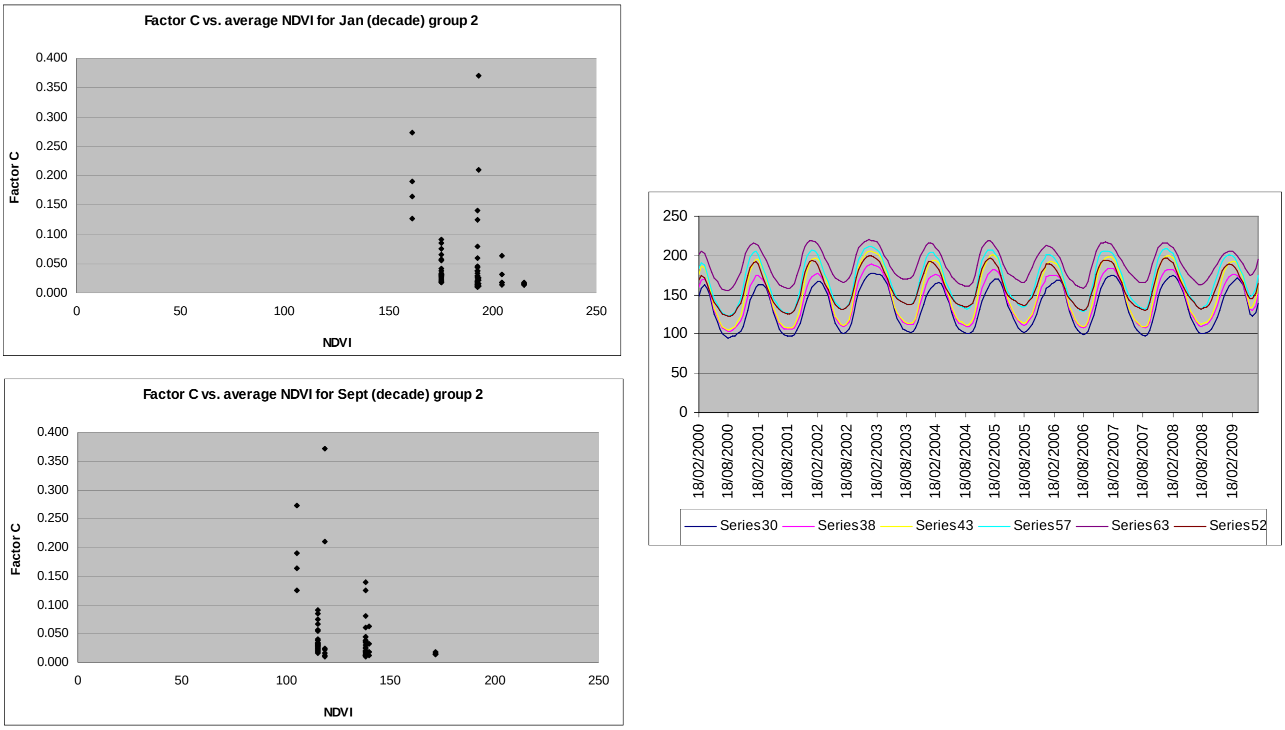

Figure 17: Relationship between factor C and NDVI for group 2.

Figure 18 shows the distribution of factor C in group 3 was observed in the range of 155 and 205 NDVI values for January and in the range of 105 and 160 for September. Similar to the first chart depicting group 1, the highest range of distribution for factor C values is clustered in the middle portion of the plots. Also this indicates that there is no high potential for soil loss within these ranges of classes. This indicates that MODIS NDVI is unable to detect factor C in the range between 160 and 185.

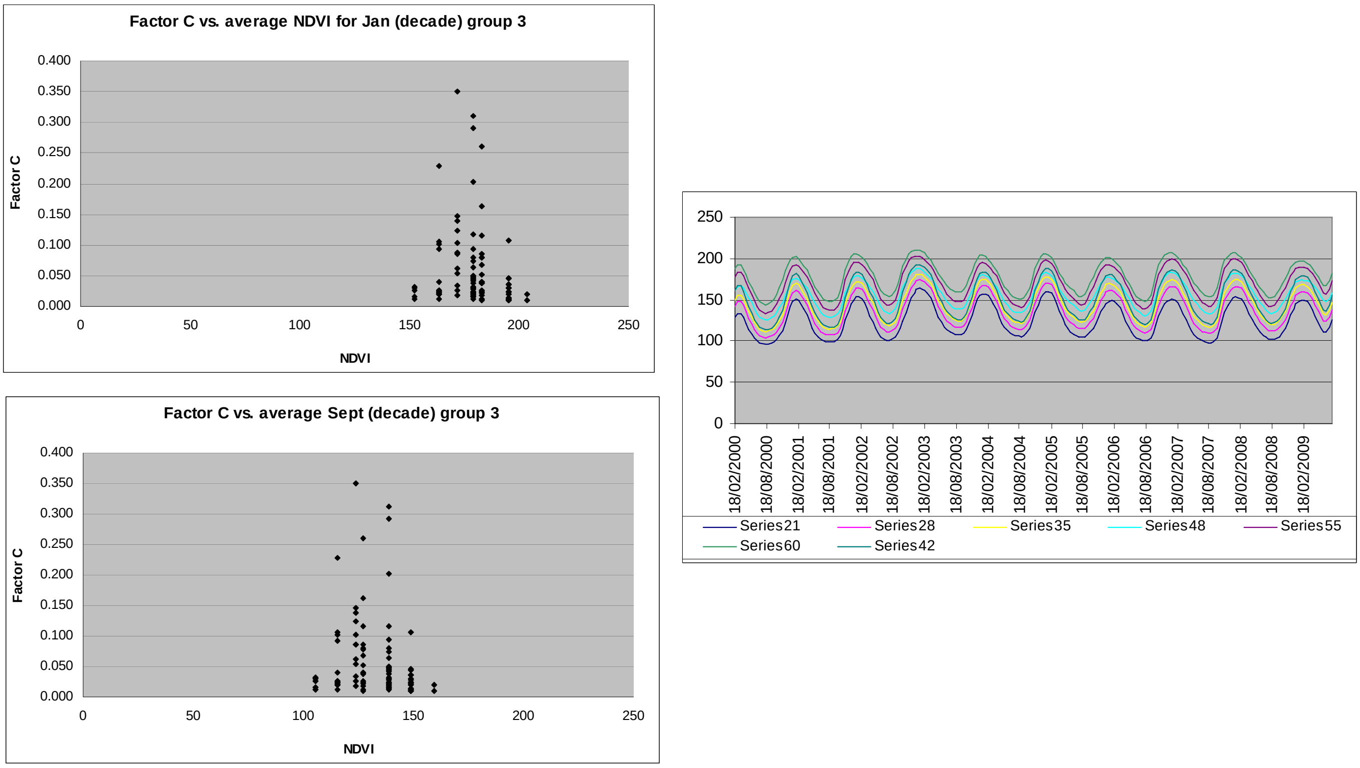

Figure 18: Relationship between factor C and NDVI for group 3.

Figure 19 shows the distribution of factor C in group 4 as observed within a range of 119 and 182 for January and between the range of 108 and 142 for September. The lowest values for factor C are found in classes on both extremes of the plot for January and the highest values are clustered in the middle of the plot. The lowest factor C values for September are observed at NDVI value of 140, indicating less potential for soil loss.

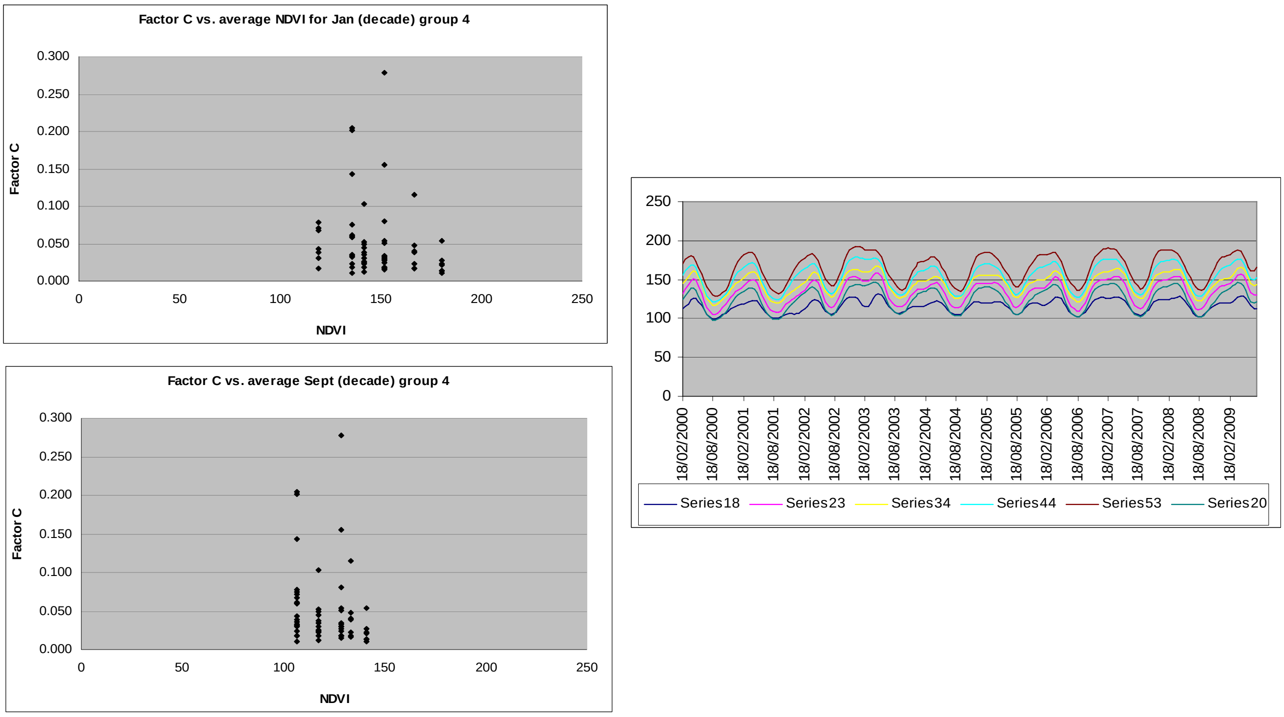

Figure 19: Relationship between factor C and NDVI for group 4.

Figure 20 shows the range of distribution for factor C in group 5 as observed between NDVI values of 135 and 198 for January and between 98 and 160 for September. Low values were observed at both extremes of the plot. Low factor C values indicate classes with less potential for soil loss. High factor C values we observed in the middle portion of the plot, the same as in figures 16-19.

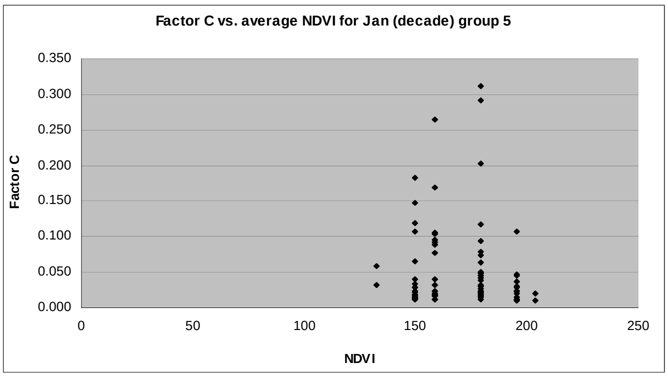

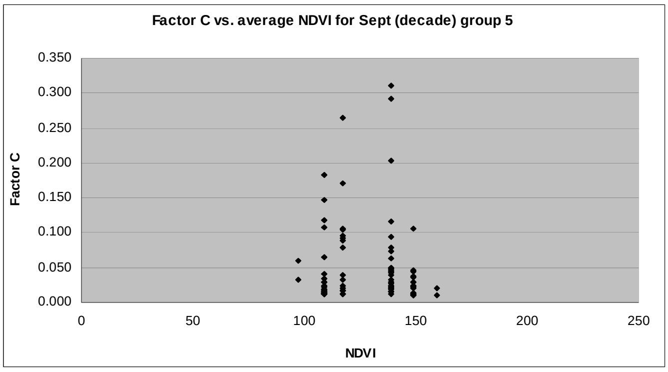

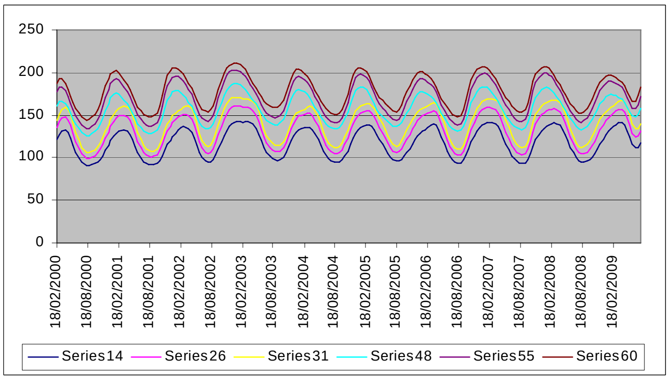

Figure 20: Relationship between factor C and NDVI for group 5.

Figure 21 shows the range of factor C in group 6 as observed between 140 at the lowest NDVI and 198 at the highest NDVI value for January and between 89 at the lowest NDVI and 129 at the highest NDVI value for September. NDVI values in this group are generally low, indicating areas with little green biomass. The classes clustered in the middle portion of the plots indicate classes with potential soil loss. Like in the previous plots, low factor C values have been observed throughout. Also the distribution of factor C in this manner indicates that MODIS NDVI is not able to detect factor C within the range of 140 to 200.

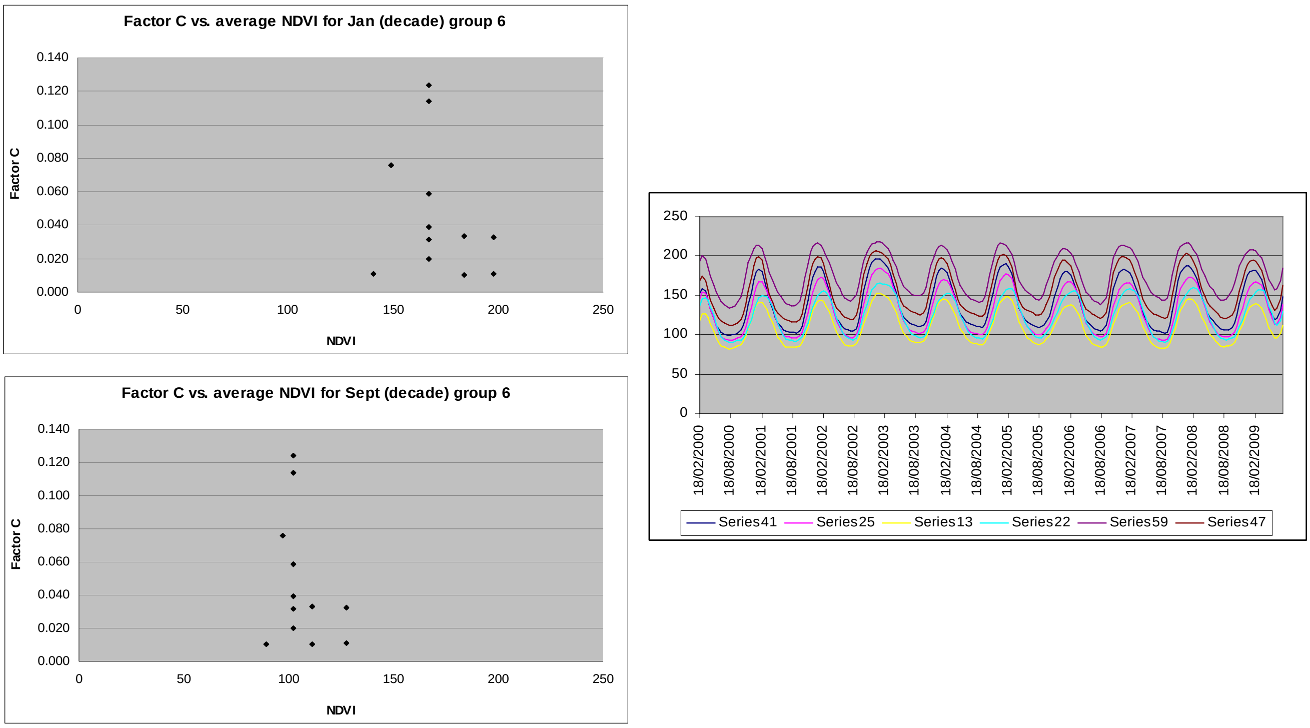

Figure 21: Relationship between factor C and NDVI for group 6.

Figure 22 shows the distribution of factor C in group 7 observed in the range of 80 to 200 for January and in the range of 85 to 175 for September. Low values were observed at both extremes of the plots, an indication of classes with less potential for soil loss.

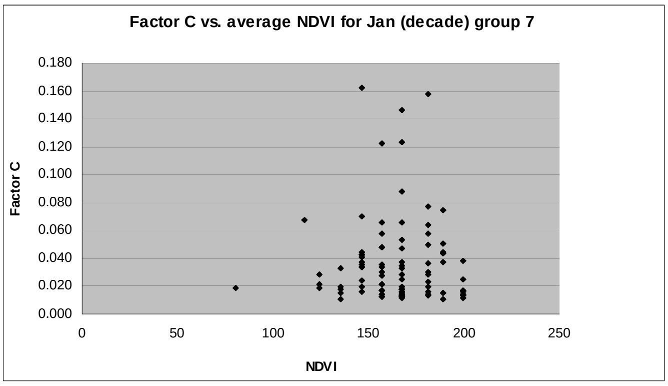

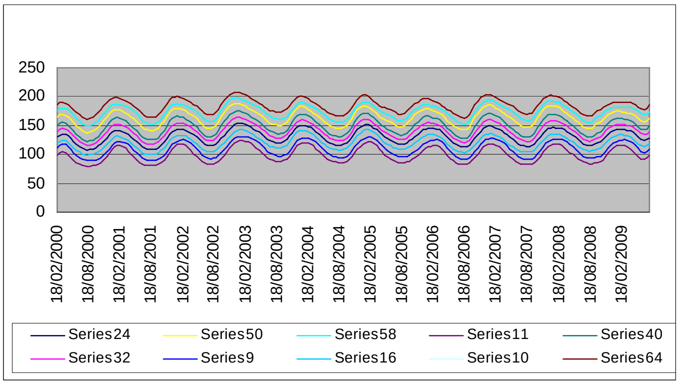

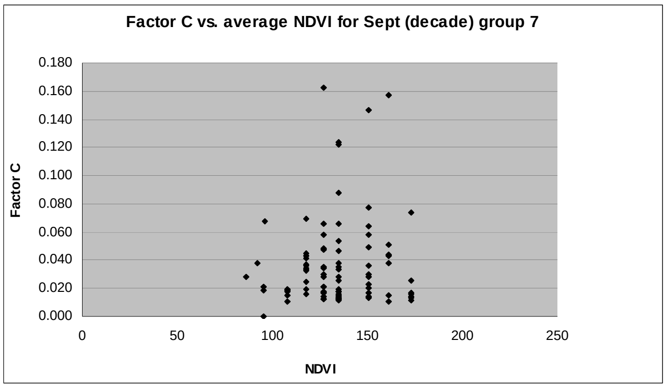

Figure 22: Relationship between factor C and NDVI for group 7.

Figure 23 shows the distribution of factor C, observed between the range of 168 and 188 for January and between 105 and 132 for September. The number of classes identified within this group was few. Factor C values within this group seem to be increasing as NDVI values increase. However this should not be a case as factor C is expected to decrease when NDVI is increasing.

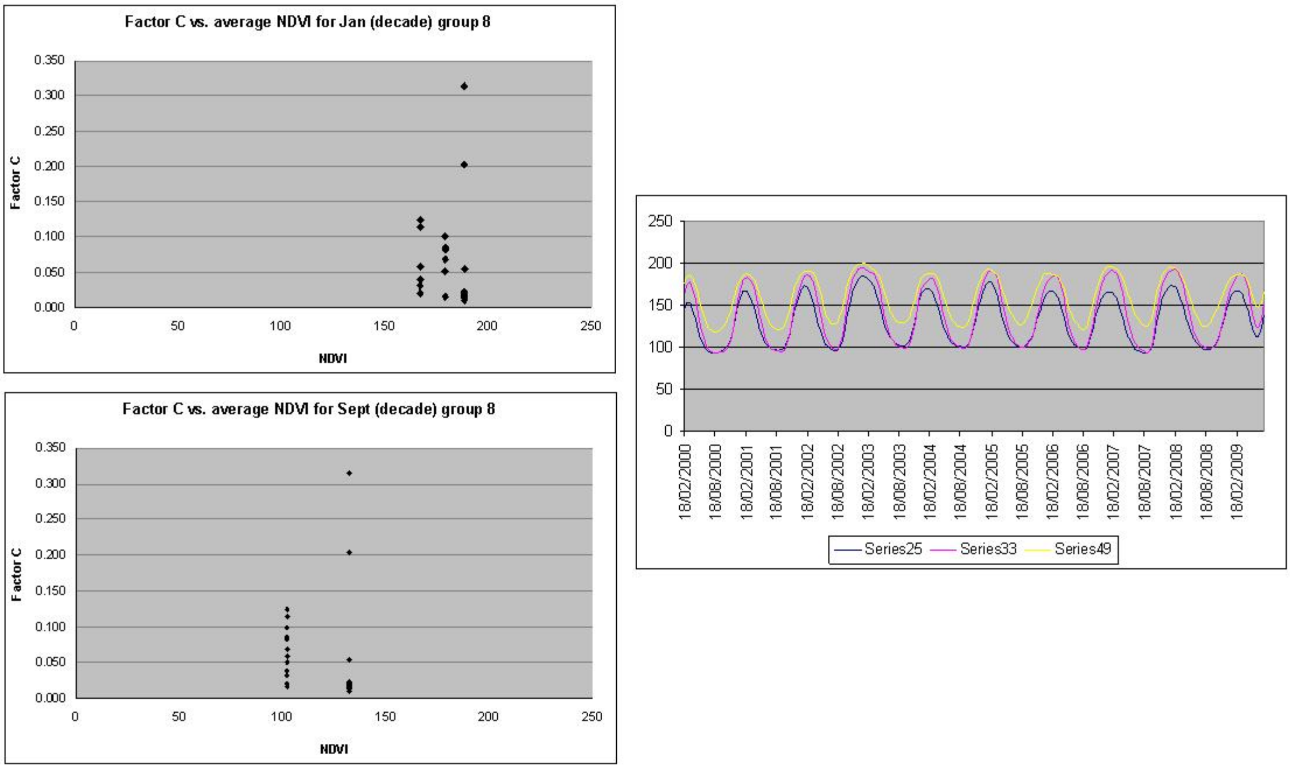

Figure 23: Relationship between factor C and NDVI for group 8.

Groups 9, 10 and 11 were not plotted as the classes represented by these groups were very few to establish a relationship with NDVI.

The relationship between groups has been assessed by comparing the behaviour of factor C values between the groups. From the visual impression of the scatter plots in figure 16 to 23, groups 1, 3, 4, 5 and 7 show a similar pattern, but at different NDVI value range. Groups 2 and 8 also show similar behaviour, although values in group 8 are not representative enough to show the variation within the group. Group 6 show an entirely different pattern as compared to other groups. Groups 9, 10, and 11 were not included in the assessment as they did not have enough representative classes to establish relations. So these groups were totally ignored.

5. Discussion

The purpose of the study was to assess the use of hyper-temporal MODIS NDVI images to estimate factor C. The hyper-temporal MODIS NDVI dataset, was used because it could provide us with both high spatial and temporal resolution, which will allow us to estimate the variation of factor C between different seasons (dry and wet). Field calculated factor C and MODIS NDVI were correlated and no relationships were observed.

Two techniques were used to reach the objective of the study. The first technique was the ISODATA clustering approach used in the unsupervised classification of the MODIS NDVI images. The analysis resulted in 65 NDVI classes that were further used to develop the field sampling scheme. MODIS pixels representing the 65 classes were arranged into groups of similar curves. Classes used in the groupings were the selected MODIS NDVI classes surrounding pixels that contained the sampled points e.g. figure 9. The grouped classes each corresponded to a factor C value. The NDVI approach was adopted from de Bie et al. (2008), and was used to distinctively distinguish the different land use / land cover types as represented by land cover classes in figure 8.

The second technique was the calculation of factor C based on field estimates of canopy cover and ground cover parameters. The range of field calculated factor C was observed between 0.0068 and 0.437 which is relatively low as compared to previous studies. In a study by Kouli et, al. (2009), factor C values were directly estimated from the NDVI image using the following formula:

$$C = e\left(-\alpha\left(\left(NDVI/\left(\beta - NDVI\right)\right)\right)\right)$$

Where α and β are unit-less parameters that determines the shape of the curve relating to NDVI and factor C, respectively. This method resulted in a significant relationship between NDVI and the estimated factor C, Kouli et al. (2009). The approach was also used in a study by Suriyaprasit et al. (2008).

In Wischmeier et al. (1978) canopy cover and ground cover were evaluated together as they are assumed to be influenced by similar interactions. However in this study canopy cover and ground cover percent were independently estimated as we assumed that the canopy above basal cover is never effective when only the plant bases are concerned (Kooiman 1987).

The resulting factor C calculated from vegetation canopy and basal cover were directly correlated to the MODIS hyper-temporal NDVI using average values for the selected months (January and September) over a 10 years period. The relationship between factor C and MODIS NDVI was assessed through graphical representation of scatter plots. The months were selected based on the NDVI profile peaks indicating low and high NDVI values as indicated in figure 14. The calculated factor C values range between 0.010 at the lowest and 0.355 at the highest. In most of the established groups, the range of factor C is mostly clustered within the middle portion of the plots as observed in figures 16 to 23. What we can summarize from these charts is that there is an inconsistency in the distribution of factor C within individual classes especially those clustered in the middle portion of the plots. Also this is an indication that MODIS NDVI is unable to detect soil loss in these classes. Low values of factor C relating to low and high NDVI values shows that there is little or no soil loss taking place in those classes.

As observed from the scatter plots in figures 16 to 23. There is no relationship between factor C and NDVI values. The result can be attributed to the low resolution of the MODIS NDVI imagery with a 250*250 m pixel size in relation to the 30*30 m quadrate at which factor C was calculated in the field (de Asis and Omasa 2007). The weak relations could also be due to the fact that the values of factor C up-scaled to the MODIS pixels were not representative of the entire class within different pixels, but were rather representative to the point of actual ground and canopy cover estimates. Moreover, assigning factor C calculated for a class unit in a certain pixel to another pixel is bias, as we are assuming that factor C for unit A in NDVI class X is the same as factor C for unit A in NDVI class Y. This assumption does not consider the heterogeneity of the landscape as well as the variability in land cover types within the different pixels.

Although NDVI is a reliable measure of vegetation greenness, it is however not able to detect the quantitative amount of protective cover, especially litter against soil loss. The NDVI index does not account for the backscattering of bare soil and rock effects van Leeuwen et al. (1996). Fragments of rock and stone cover characterises most part of the study area and contributes about 29% of the ground cover sub-factor. The percent of stone cover was found to be relatively high in relation to litter and bare soil, although basal cover contributes the highest percent to the ground cover estimates. In figure 12 of the ALOS classification, class B represents factor C for areas with a high percent of stone cover. It should be noted that the ALOS classes in figure 12 are not land cover / land use specific and that they are representative of a complex of land cover parameters. The percent distribution of stone cover from field estimated ground cover is presented in figure 24 below. Stone cover contributes about 29 % of the ground cover estimates. Therefore, further studies should consider using different indices to assess the different parameters that accounts for ground cover effects, especially the stone cover factor.

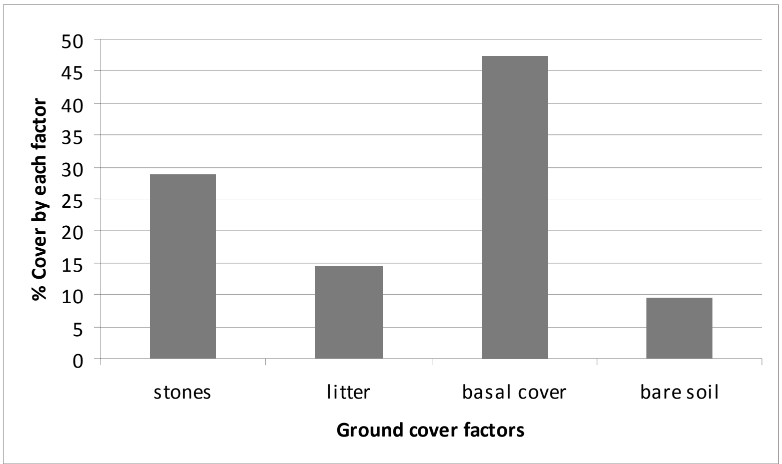

Figure 24: Percent distribution of ground cover factors

Field data collection was carried out during the dry season, thus canopy cover estimations were low as compared to the average NDVI values over the 10 years period. In addition, NDVI has limited capabilities to quantify the total ground cover, which includes all non-photosynthetic materials that are important in the estimation of factor C. Due to the absence of contrast in the reflectance between the red and the near infrared wavelengths in dry vegetation, NDVI is not able to detect (de Asis and Omasa 2007) the variation in factor C.

In a study conducted by Patric (1976), it was found that soil loss at the rates ranging between 0.07 and 0.11 t ha^{-1} y^{-1} can occur even in undisturbed forests having a high percentage of canopy and litter cover. Therefore we can assume that low values obtained for field calculated factor C, mean that there is no potential for soil loss in the study area due to less bare soil exposure and high ground cover parameters. But then it could also mean that the range of low factor C values was obtained in areas of high vegetation and ground cover factors (de Asis and Omasa 2007).

In relation to the cover factor C, Wischmeier et al. (1978) suggested that, factor C as a weighted average is based on the rainfall erosivity. The rainfall erosivity can be approximated by multiplying the C values by the seasonal R values, summing the products (CR) and dividing by the annual R. However due to the unavailability of rainfall data, this was not applied, but should be considered in further studies looking into developing methods of estimating factor C, de Asis et al. (2007).

Vegetation cover in the Crete Island is dominated by mountain phragana and grass steppe amongst others. However it is assumed that the present vegetation cover types represent centuries of land degradation and soil erosion. But in a study by Rackham and Moody (1996) it was found that the modern vegetation types in the study area appear to be relatively resistant to change. Vegetation is more likely to have been influenced by the land use and management practices applied. The types of vegetation pattern and its environment (Sarris et al. (2005) was found to be rather difficult to detect with satellite images. This is mainly due to the complexity of the terrain and the land surface that provided obstacles in the clear discrimination of land uses and habitat types. Little or no signs of soil loss were observed in the field, which could quantify the assumed current status of soil loss as reported in a study by Kouli et, al. (2009).

6. Conclusions and recommendations

The purpose of the study was to assess the usefulness of MODIS NDVI in estimating factor C. The objective was answered by assessing the relationships between factor C and MODIS NDVI values and the results showed that there is no relationship between factor C and MODIS NDVI. From what was presented it can be concluded that MODIS NDVI is not able to detect factor C, therefore further studies should consider looking into possibilities of using datasets of high spatial and temporal resolution, as they might yield better and accurate timely estimates of soil loss. Also further studies in this area should look into the possibility of using different vegetation indices that uses the full spectral range of wavelength, as they are able to detect not only green vegetation but also non-green cover types apart from green vegetation.

7. References

Ali, A. (2009). Comparison of strengths and weaknesses of NDVI and landscape - ecological mapping techniques for developing an integrated land use mapping approach : a case study of the Mekong delta, Vietnam. Enschede, ITC**:** 56.

Alodos, C., Y. Pueyo, et al. (2004). "Variations in landscape patterns and vegetation cover between 1957 and 1994 in a semiarid Mediterranean ecosystem." Landscape ecology **19**(5): 543-559.

Andel, T. H. v., E. Zangger, et al. (1990). "Land Use and Soil Erosion in Prehistoric and Historical Greece." Journal of Field Archaeology **17**(4): 379-396.

Arianoutsou, M. (2001). "Landscape changes in Mediterranean ecosystems of Greece: implications for fire and biodiversity issues." Journal of Mediterranean Ecology **2**: 165-178.

Beltran-Abaunza, J. M. (2009). Method development to prepare from hyper - temporal images remote sensing RS - based change maps. Enschede, ITC**:** 53.

CEH. (2009). "CORINE Land Cover map of the UK." Retrieved 15 September 2009, from http://www.ceh.ac.uk/sci_programmes/BioGeoChem/CORINELandCoverMap.html.

Damen, M. C. J. (1991). Introduction to Soil Erosion by Water. Enschede, ITC**:** 50.

de Asis, A. M. and K. Omasa (2007). "Estimation of vegetation parameter for modeling soil erosion using linear Spectral Mixture Analysis of Landsat ETM data." ISPRS Journal of Photogrammetry and Remote Sensing **62**(4): 309-324.

De Bie, C., M. Khan, et al. (2008). "Hypertemporal Image Analysis for Crop Mapping and Change Detection." ITC Academic Output.

De Bie, C. A. J. M. (2005). "Assessment of soil erosion indicators for maize-based agro-ecosystems in Kenya." Catena **59**(3): 231-251.

de Bie, C. A. J. M., J. P. Bouma, et al. (2000). Comparative performance analysis of agro - ecosystems. ITC Dissertation;75. Enschede, ITC**:** 232.

Gitas, I., K. Douros, et al. (2009). "Multi-temporal soil erosion risk assessment in N. Chalkidiki using a modified USLE raster model." EARSeL Proceedings **8**(1): 40-52.

Gumiere, S., Y. Le Bissonnais, et al. (2009). "Soil resistance to interrill erosion: Model parameterization and sensitivity." Catena.

Hill, J., P. Hostert, et al. (1998). "Monitoring 20 years of increased grazing impact on the Greek island of Crete with earth observation satellites." Journal of Arid Environments **39**(2): 165-178.

http://www.alos-restec/. (2009). "ALOS Data." Retrieved August 2009, 2009, from http://www.alos-restec.jp/aboutalos5_e.html.

http://www.landcover.org/data/ndvi/. (1997). "MODIS Normalized Difference Vegetation Index." Retrieved 02 February, 2010, from http://www.landcover.org/data/ndvi/.

http://www.omafra.gov.on.ca/. (17 August 2009). "Ministry of Agriculture Food and Rural Affairs." Retrieved 1 February, 2010, from http://www.omafra.gov.on.ca/.

http://www.yale.edu/. (2010). "Unsupervised Classification algorithms." Retrieved 09 February, 2010.

Institute of Water Research. (2007). "RUSLE - an online soil erosion assessment tool." Retrieved 23 January, 2010, from http://www.iwr.msu.edu/rusle/about.htm.

Karlsen, S. R., A. Tolvanen, et al. (2008). "MODIS-NDVI-based mapping of the length of the growing season in northern Fennoscandia." International Journal of Applied Earth Observation and Geoinformation **10**(3): 253-266.

Karydas, C. G., T. Sekuloska, et al. (2009). "Quantification and site-specification of the support practice factor when mapping soil erosion risk associated with olive plantations in the Mediterranean island of Crete." Environmental Monitoring and Assessment **149**(1-4): 19-28.

Kooiman, A. (1987). The Factor C: Relations between Landcover and Landuse, and Aspects of Soil Erosion, Specifically for the Upper Komering Catchment, South Sumatra, Indonesia. Department of Rural and Landecology Survey. Enschede, The Netherlands, International

Institute for Aerospace Surveys and Earth Sciences (ITC), Land Resources and Rural Development. **Msc:** 129.

Kouli, M., P. Soupios, et al. (2009). "Soil erosion prediction using the Revised Universal Soil Loss Equation (RUSLE) in a GIS framework, Chania, Northwestern Crete, Greece." Environmental Geology **57**(3): 483-497.

López-Bermúdez, F., A. Romero-Díaz, et al. (1998). "Vegetation and soil erosion under a semi-arid Mediterranean climate: a case study from Murcia (Spain)." Geomorphology **24**(1): 51-58.

Lorent, H., C. Evangelou, et al. (2008). "Land degradation and economic conditions of agricultural households in a marginal region of north Greece." Global and Planetary Change **64**(3-4): 198-209.

Mainam, F. l. (2000). Modelling soil erodibility in the semiarid zone of Cameroon. Faculty of Sciences. Ghent, University of Ghent. **Doctor (PhD) in Earth Sciences (thesis):** 282.

Merritt, W. S., R. A. Letcher, et al. (2003). "A review of erosion and sediment transport models." Environmental modelling and software **18**: 761-799.

Nyakatawa, E. Z., K. C. Reddy, et al. (2001). "Predicting soil erosion in conservation tillage cotton production systems using the revised universal soil loss equation (RUSLE)." Soil and Tillage Research **57**(4): 213-224.

Ouled Belgacem, A. and V. Papanastasis (1995). "Impact of grazing practices on rangeland vegetation of western Crete." Cahiers Options Mediterraneennes (CIHEAM).

Patric, J. H. (1976). "Soil erosion in the eastern forest." Forestry **10**(126): 671-677.

Pettorelli, N., J. O. Vik, et al. (2005). "Using the satellite-derived NDVI to assess ecological responses to environmental change." Trends in Ecology & Evolution **20**(9): 503-510.

Pueyo, Y., C. Alados, et al. (2006). "Determinants of land degradation and fragmentation in semiarid vegetation at landscape scale." Biodiversity and Conservation **15**(3): 939-956.

Saavedra, C. (2005). Estimating spatial patterns of soil erosion and deposition in the andean region using geo-information techniques. Water Resources. Enschede, Internation Institute for Geo-Information Science and Earth Observation. **PhD Thesis:** 244.

Sarris, A., S. Karakoudis, et al. (2005). "Study of the morphological attributes of crete through the use of remote sensing techniques." IASME Transactions **2**(6): 1043-1051.

Sarris, A., M. Maniadakis, et al. (2005). Studying Land Use Patterns in Crete Island, Greece, Through a Time Sequence of Landsat Images and Mapping Vegetation Patterns. WSEAS International Conference on Environment, Ecosystems and Development. Venice, Italy**:** 112-119.

Scarrott, R. G. (2009). Extracting gradient boundaries using hyper - temporal imaging analysis : progress towards a tool for gradient analysis. Enschede, ITC**:** 91.

Shrestha, D., J. Zinck, et al. (2004). "Modelling land degradation in the Nepalese Himalaya." Catena **57**(2): 135-156.

Suriyaprasit, M. and D. P. Shrestha (2008). "Deriving land use and canopy cover factor from remote sensing and field data in inaccessible mountainous terrain for use in soil erosion modelling." In: ISPRS 2008 : Proceedings of the XXI congress : Silk road for information from imagery : the International Society for Photogrammetry and Remote Sensing, 3-11 July, Beijing, China. Comm. VII, SS-7. Beijing : ISPRS, 2008. pp. 1747-1750.

van Leeuwen, W. J. D. and A. R. Huete (1996). "Effects of standing litter on the biophysical interpretation of plant canopies with spectral indices." Remote Sensing of Environment **55**(2): 123-138.

Verheijen, F., R. Jones, et al. (2009). "Tolerable versus actual soil erosion rates in Europe." Earth Science Reviews.

Wischmeier, W. and D. Smith (1978). Predicting Rainfall Erosion Losses: a guide to conservation planning (Agriculture Handbook, No. 537). US Department of Agriculture. Washington, DC**:** 58.

Yang, X. and Z. Liu (2005). "Using satellite imagery and GIS for land-use and land-cover change mapping in an estuarine watershed." International Journal of Remote Sensing **26**(23): 5275-5296.

8. Appendix

8.1. Land cover field survey form

A.

Cluster no.: ………………	**Date: …………………**
Name of observer (s): ……………………………………………….	

B.

Day/Sample No.: ……………	**Sample size: ………………….**
X-Coordinates:	**Corine classes: ……………….**
Y-Coordinates:	**SPOT: classes: ……………….**
	MODIS classes: ………………

C.

Ground cover:	**%**			**Erosion features of bare soil**	**BB scale***	**%**
Stones				Pre-rills**		
Litter				Rills**		
Basal cover				Sheet wash**		
Bare soil						
Water						
Total	**100%**					
Roughness ***	**S**	**M**	**R**			
Infiltration rate						
Soil colour						
Texture						

D.

Vegetation structure (drawing)	Vegetation composition vertical

Height (m)

10										
9										
8										
7										
6										
5										
4										
3										
2										
1										
0	10	20	30	40	50	60	70	80	90	100

% cover

E.

Properties vegetation layer	1	2	3	4	5
% cover					
Biomass density*					
Photo nos.:					
Dominant spp.					